REVIEW

doi:10.1038/nature22012

Quantum design of photosynthesis for bio-inspired solar-energy conversion

Elisabet Romero[1], Vladimir I. Novoderezhkin[2] & Rienk van Grondelle[1]

Photosynthesis is the natural process that converts solar photons into energy-rich products that are needed to drive the biochemistry of life. Two ultrafast processes form the basis of photosynthesis: excitation energy transfer and charge separation. Under optimal conditions, every photon that is absorbed is used by the photosynthetic organism. Fundamental quantum mechanics phenomena, including delocalization, underlie the speed, efficiency and directionality of the charge-separation process. At least four design principles are active in natural photosynthesis, and these can be applied practically to stimulate the development of bio-inspired, human-made energy conversion systems.

Humankind is facing an energy challenge: the urgent need to find a clean source of energy that is able to fulfil our growing demands for energy. Solar energy is the most promising such source because it is widely available and is clean, safe and renewable. Photosynthesis is the natural process by which solar photons are converted into chemical energy to be used by organisms (plants, algae and photosynthetic bacteria) to live and reproduce. Therefore, photosynthesis is the link between the Sun and life on Earth[1].

The overall process of oxygenic photosynthesis is described by the equation: $6\,H_2O + 6\,CO_2 + \text{sunlight} \rightarrow C_6H_{12}O_6 + 6\,O_2$. The most crucial reactions of photosynthesis therefore involve the oxidation of water to oxygen and the reduction of carbon dioxide to glucose ($C_6H_{12}O_6$), which are driven by energy from sunlight.

During the early steps of photosynthesis, specialized complexes that contain pigments and proteins (pigment–protein complexes) absorb, transfer and convert energy from sunlight into the chemical energy that is needed to power the biochemistry of life. The absorption of light takes place on a timescale of femtoseconds (1 fs = 10^{-15} s), and it is efficient owing to the use of pigments with large absorption coefficients, as well as to the high density of pigments in the photosynthetic complexes — a density that is unattainable in solution without the complete quenching of the absorbed energy[2]. The transfer and conversion of the absorbed excitation energy needs to be ultrafast and irreversible because the pigments are able to conserve solar excitation energy for only a few nanoseconds (1 ns = 10^{-9} s). Consequently, the energy has to be transferred and converted in a few tens of picoseconds (1 ps = 10^{-12} s). In this way, almost all of the energy that is absorbed from sunlight is converted to electrochemical energy by photosynthetic complexes. Photosynthesis therefore holds the key to the efficient use of solar energy by humans using abundant and renewable materials.

Advances in our understanding of photosynthesis have revealed the mechanisms that promote its success in unprecedented detail, enabling researchers to apply the discovered principles to the design of human-made energy conversion systems. In this Review, we focus on the charge-separation process in photosynthetic reaction centres in which solar excitation energy is converted into a stable pair of separated charges with close to 100% efficiency. We describe the advances that have been achieved by combining experimental and theoretical methods, with a focus on the quantum nature of charge separation, and classify this understanding according to four design principles. We conclude with a discussion on how to apply these principles in practice to contribute to accomplishing the long-term goal of affordable, sustainable and efficient solar-to-fuel energy conversion. It should be noted that a commercially viable human-made energy conversion system must fulfil simultaneously the following requirements: high efficiency, long-term stability, low cost, scalability and the use of renewable materials. Because the issue of efficiency is a considerable bottleneck, we focus on the lessons that can be learnt from nature to fulfil this requirement.

Reaction centres

The concept of the photosynthetic reaction centre originated as an interpretation of the pioneering experiments by Robert Emerson and William Arnold in 1932 (ref. 3), which showed that the exposure of green algae to short saturating flashes of light reduced only one molecule of carbon dioxide per 2,500 molecules of chlorophyll. Louis N. M. Duysens established experimentally that most chlorophyll molecules function as light harvesters by absorbing and transferring excitation energy to a unique subset of chlorophylls in which solar excitation energy is converted into useful chemical work. He then proposed that this special group of chlorophylls formed the reaction centres[4].

Here, we will focus on the type II reactions centres that are found in purple bacteria (the bacterial reaction centre) and oxygen-evolving organisms such as cyanobacteria, algae and plants (the photosystem II (PSII) reaction centre). Both of these reaction centres are pigment–protein complexes that are embedded in the photosynthetic membrane. Whereas the bacterial reaction centre binds bacteriochlorophyll *a* and bacteriopheophytin *a*, the PSII reaction centre binds chlorophyll *a* and pheophytin *a*. The structures of both the bacterial reaction centre[5,6] and the cyanobacterial PSII reaction centre[7–9] have been resolved to atomic resolution by X-ray crystallography (Fig. 1), and they are similar. At the centre, each contains four bacteriochlorophyll or chlorophyll molecules, two bacteriopheophytin or pheophytin molecules and two quinone molecules, which are arranged in two quasi-symmetric branches. The bacterial reaction centre also contains one carotenoid molecule and the PSII reaction centre contains two peripheral chlorophyll *a* molecules called chlorophyll z, which are located at opposing sides of the complex, as well as two carotenoids that sit between each chlorophyll z and the centre of the complex. The pigments are non-covalently bound to two protein domains that are labelled A and B (or L and M) in the bacterial reaction centre and D1 and D2 in the PSII reaction centre. Each pigment

[1]Department of Physics and Astronomy, Faculty of Sciences, VU University, 1081 HV Amsterdam, the Netherlands. [2]A. N. Belozersky Institute of Physico-Chemical Biology, Moscow State University, Leninskie Gory, 119992 Moscow, Russia.

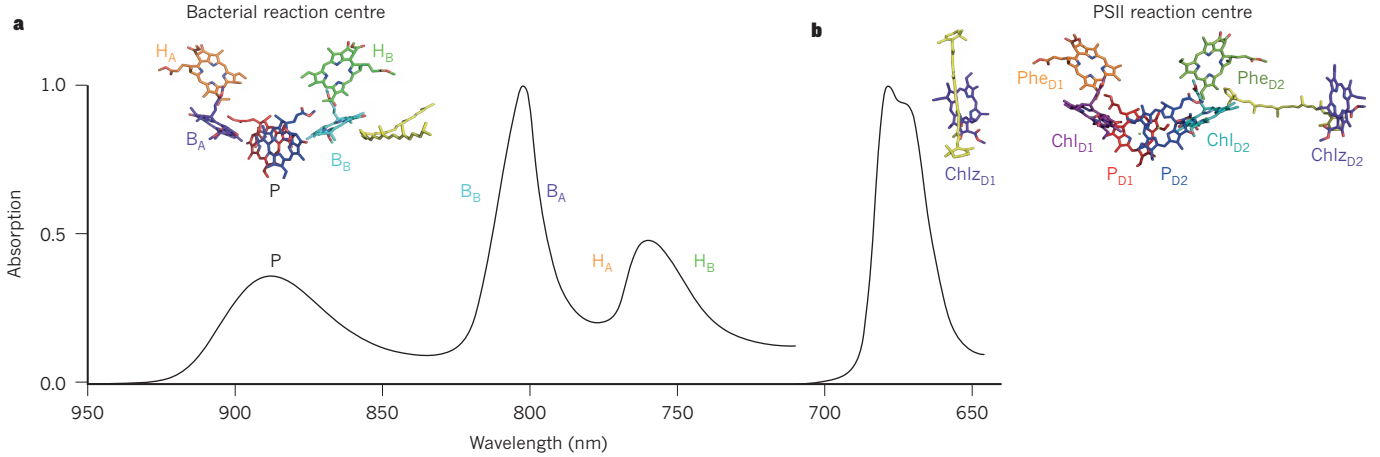

Figure 1 | Absorption spectra and X-ray structure of the bacterial reaction centre and the PSII reaction centre. **a**, The absorption spectrum of the bacterial reaction centre of *Rhodobacter sphaeroides* at 77 K is shown with the X-ray crystal structure of the complex (adapted from ref. 6). The locations of the pigments in the X-ray structure are highlighted and a band in the absorption spectrum has been assigned to each pigment. The carotenoid molecule is shown in yellow. The spectrum has been normalized to 1 at its absorption maximum. **b**, The 77 K absorption spectrum of the PSII reaction centre of spinach (*Spinacia oleracea*) is displayed with the X-ray crystal structure of the complex (adapted from ref. 9). The locations of the pigments in the X-ray structure are highlighted. The carotenoid molecules are shown in yellow. Owing to spectral congestion, the assignment of absorption bands to the pigments cannot be shown here (see Box 1). The spectrum has been normalized to 1 at its absorption maximum.

is named after its position in a specific branch. In the bacterial reaction centre, with the exception of the two central bacteriochlorophyll molecules that are together known as P (special pair), these pigments are called B_A, B_B, H_A and H_B (in which B represents bacteriochlorophyll and H represents bacteriopheophytin); in the PSII reaction centre, the pigments are called P_{D1}, P_{D2}, Chl_{D1}, Chl_{D2}, Phe_{D1}, Phe_{D2}, $Chlz_{D1}$ and $Chlz_{D2}$ (in which P, Chl and Chlz are chlorophylls and Phe is pheophytin).

The reaction centre pigments absorb sunlight, which is received directly or through light-harvesting antennas[10], and have an important role in energy transfer and electron-transfer processes in the reaction centre. The protein component of the reaction centre (the matrix) maintains the pigments in certain positions in the complex and provides a specific environment for each, which enables the pigment–protein interactions that modulate the energy of the pigments to be controlled. In this sense, the protein acts as a 'smart' matrix. Each pigment therefore has a particular excited-state energy, which is determined by the pigment's interactions with the local environment. Furthermore, owing to the close proximity of the pigments, interactions between pigments are also present. The most prominent consequence of pigment–pigment interactions is the formation of excitons[11], which are collective excited states in which the excitation is shared by (or delocalized over) more than one pigment (Frenkel excitons[12] or bound electron–hole pairs). The pigment–protein complex is also continuously exposed to the fast nuclear motions of the atoms it contains (dynamic disorder) as well as to the slow motions of the protein matrix (static disorder). Dynamic disorder refers to intramolecular vibrations of the pigments and to collective pigment or protein vibrations, namely phonons. Static disorder generates distinct protein configurations with specific pigment–protein and pigment–pigment interactions. As a consequence, at any moment, the sample ensemble contains a distribution of energetically different complexes.

Charge separation

The charge-separation process converts excitation energy into a stable charge-separated state. In isolated reaction centres that lack quinones, the energy of the system relaxes to the lowest energy state in a few hundred femtoseconds[13]. In the primary electron transfer reaction, the lowest energy state is converted into a charge-transfer state that is characterized by the localization of the electron and the hole on adjacent molecules. In the secondary electron-transfer reaction, the final charge-separated state ($P^+H_A^-$ in the bacterial reaction centre and $P_{D1}^+Phe_{D1}^-$ in the PSII reaction centre) is generated in a few tens of picoseconds. Notably, further irreversible electron-transfer reactions occur in reaction centres in their native membranes; for reviews, see ref. 14 (bacterial reaction centre) and refs 15–17 (PSII reaction centre). It has been established that only one branch of pigments is active in charge separation: the A branch in the bacterial reaction centre[18] and the D1 branch in the PSII reaction centre[15].

The most suitable experimental methods with which to study the energy levels (or energy landscape) and the dynamics of the ultrafast events in photosynthetic complexes are spectroscopic techniques[19]. A variety of steady-state spectroscopic techniques that are sensitive to certain features (indicated by parentheses) are available: absorption spectroscopy (energy of the absorbing states), fluorescence spectroscopy (energy of the lowest energy-emitting state), linear dichroism and circular dichroism (pigment interactions and orientations), triplet-minus-singlet spectroscopy (energetic position of the triplet state and of the singlet state on which the triplet is formed) and Stark spectroscopy (charge-transfer character of excited states). To follow the dynamics of charge separation, time-resolved spectroscopic techniques are applied. For instance, transient absorption spectroscopy[20] (also referred to as pump–probe spectroscopy) uses two ultrashort laser pulses, the excitation (or pump) pulse and a white-light continuum that serves as the probe pulse. By temporally separating the probe pulse from the pump pulse, the dynamics of the energy transfer or electron transfer that is initiated by the pump can be observed through changes in absorption that are reported by the probe at certain points after excitation — that is, as a function of the delay between the pump and probe. Similarly, time-resolved fluorescence can be measured at various points after laser pulse excitation. Another time-resolved technique, two-dimensional electronic spectroscopy[21], which uses three laser pulses to generate the required response in the sample, has been applied to investigate the presence and role of quantum coherence and delocalization in energy-transfer or electron-transfer processes.

Although spectroscopic techniques provide a vast amount of information about the energy landscape and dynamics of photosynthetic complexes, the high density of pigments in such complexes, in which several pigments absorb at similar energies, greatly complicates the assignment of absorption bands to specific pigments (or combinations of pigments) that were identified in the X-ray crystal structure. To overcome this spectral congestion, modified reaction centres with tailored pigment–protein or pigment–pigment interactions have been generated, including ones

in which pigments are removed[22] or replaced[23], and some with single amino-acid mutations in the protein[24]. By comparing the spectroscopic response of the wild-type complex to that of the modified complex, the excited-state properties of the targeted pigments can be assigned.

Theoretical modelling of experimental data has proved to be successful in extending our understanding of the function of photosynthetic complexes. Such modelling assists in the interpretation of experimental data and provides predictive power. It is also capable of simulating situations that are inaccessible to experiments, which enables researchers to go beyond the information that is contained in the experimental data. Here, our discussion is restricted to (modified) Redfield theory[25], which facilitates the simultaneous and quantitative explanation of all spectral responses and dynamics of photosynthetic complexes using just one function that describes the coupling between pigments, the coupling of the electronic excited states (or excitons) of the pigments to the nuclear motion (including the phonon modes of the pigment–protein matrix and the high-frequency intramolecular vibrations of the pigments) and the static disorder. Once the spectral density of the exciton–phonon coupling has been specified (through experiments or first–principles calculations), the simultaneous and quantitative modelling of various steady-state and time-resolved spectral responses becomes possible. This permits one to build a unified physical picture that is able to explain both the steady-state spectra (using realistic line shapes) and the dynamics of excitations that emerge from transient absorption spectroscopy, time-resolved fluorescence spectroscopy and two-dimensional electronic spectroscopy, which determine the pathways and timescales of energy transfer and electron transfer in photosynthetic complexes.

The first step towards comprehending charge separation is the analysis of the absorption spectrum. Despite similarities in their structure, the absorption spectra of the bacterial reaction centre and the PSII reaction centre in the Q_y region, in which the energy transitions (or absorption bands) that are involved in charge separation are found, are very different (≈700–950 nm and ≈650–700 nm, respectively) (Fig. 1). Whereas the bacterial reaction centre presents three distinct absorption bands, the PSII reaction centre displays only one band. This variation in the energy landscape of the two systems is the result of a small structural difference in the central pigments of each (special pair P in the bacterial reaction centre and P_{D1} and P_{D2} in the PSII reaction centre). Although the distance between the pigment centres is similar in both (7.8 Å in the bacterial reaction centre[6] versus 8.1 Å in the PSII reaction centre[9]), the relative orientation of the pigments is different. In the bacterial reaction centre, the orientation of the P pigments enables a good overlap of the central bacteriochlorophyll molecules, but in the PSII reaction centre, the relative orientation of P_{D1} and P_{D2} gives rise to a lower degree of overlap[6,9,26]. Consequently, in the bacterial reaction centre, the central bacteriochlorophyll molecules form a strongly coupled dimer (the special pair P) and the other pigments (B_A, B_B, H_A and H_B) are regarded as being mostly monomeric owing to the large energy gap between them that considerably exceeds the pigment–pigment couplings. By contrast, in the PSII reaction centre, the energy gaps between the pigments are relatively small. As a result, all pigments (or combinations of pigments) absorb at similar energies and only one absorption band — which contains several sub-bands — is observed. These differences in energy landscape give rise to distinct charge-separation dynamics. The bacterial and PSII reaction centres share the capacity to perform ultrafast and efficient light-induced charge separation. However, a considerable and physiologically relevant difference is the fact that the PSII reaction centre is able to drive light-induced water oxidation, which requires an oxidation–reduction midpoint potential of at least 0.93 V at pH 5 (ref. 27), whereas the bacterial reaction centre is unable to do so. (The oxidation–reduction midpoint potential of the generated final cation is 1.1–1.3 V for the PSII reaction centre[15,28] and 0.50 V for the bacterial reaction centre[29].)

Charge separation in the bacterial reaction centre

In the bacterial reaction centre, the special pair P is always the lowest excited energy state in the system. On excitation, the electronic energy therefore relaxes to form the P excited state (P*). The subsequent transfer of an electron to B_A in 3 ps, and from B_A to H_A in 1 ps, generates the final charge-separated state $P^+H_A^-$ in the sequence[14,30] $P^* \rightarrow P^+B_A^- \rightarrow P^+H_A^-$. Experiments on a mutant bacterial reaction centre provided evidence for another ultrafast charge-separation pathway, in which the excited state of B_A (B_A^*) can act as the primary electron donor without the involvement of P* (ref. 31). However, *in vivo*, this alternative pathway does not have a considerable role because the energy level of B_A is too high for it to receive excitation energy from the light-harvesting complexes. Excitation of the P band in a mutant bacterial reaction centre showed that charge separation does not start from a vibrationally relaxed P*. Broadband transient absorption spectroscopy experiments revealed that P* is coupled to nuclear vibrations which, in turn, give rise to long-lived oscillations in signal amplitude (also referred to as quantum beats) that correspond to a coherent motion of the excited-state vibrational wave packet in the P* potential[32] (Box 1). Remarkably, in native and H_A-modified bacterial reaction centres, a wave-packet-like motion could also be observed in the absorption band of the primary photoproduct $P^+B_A^-$ (ref. 33). The amplitude of coherent oscillations in both the P* and $P^+B_A^-$ bands is considerable during primary charge separation, which means that the physics of charge separation is more complicated than just tunnelling between two diabatic electronic states with equilibrated nuclear modes. The simplest scheme (Box 1) implies a strong mixing of the vibrational wavefunctions of the P^*B_A and $P^+B_A^-$ states, which enables the coherent motion of the electron-vibrational wave packet between the two potentials. The Fourier spectrum of the oscillations in the stimulated emission of the reactant P^*B_A and in the absorption of the product $P^+B_A^-$ contains two modes (30 cm^{-1} and 130 cm^{-1}), with a notable increase of the low-frequency 30 cm^{-1} mode in the photoproduct. The observation of oscillatory components also in the H_A band supports the proposal that the 30 cm^{-1} mode results in the coherent formation of the final charge-separated state $P^+H_A^-$.

To describe the observed spectral evolution, electron-vibrational dynamics have been modelled using a density matrix equation with the Redfield superoperator in the basis of electron-vibrational states. The model includes two diabatic states: an excited state P* and a charge-transfer state $P^+B_A^-$, each of which are coupled to two collective nuclear modes[34]. The mixing of diabatic states (with different displacements along each of the two nuclear coordinates) leads to a complicated potential energy surface that determines the dynamics of the excited-state wave packet. The model results in a quantitative fit of the experimental kinetics. The configuration of the two vibrational coordinates that are involved has an essential role in establishing the high efficiency of charge separation for both coherent and incoherent excitation. In particular, strong coupling to the 130 cm^{-1} mode enables effective electron transfer from the primary donor P* to the photoproduct $P^+B_A^-$, whereas strong coupling of the product state to the 30 cm^{-1} mode causes movement of the $P^+B_A^-$ part of the wave packet away from the crossing point, which therefore stabilizes the charge-separated state (Box 1).

Charge separation in the PSII reaction centre

In the PSII reaction centre, the primary electron donor from which charge separation starts is conventionally referred to as P680 (pigment that absorbs at 680 nm) (ref. 35). The extent of excitonic interactions between the pigments at the centre of the PSII reaction centre has long been debated. Some authors propose that these interactions can be neglected and that P680 should be viewed as a weakly coupled dimer of the central P_{D1} and P_{D2} chlorophyll molecules[36,37], whereas others suggest that the interactions between all six chlorins should be taken into account[38–40] and that the central part of the PSII reaction centre should be viewed as a weakly coupled multimer of four chlorophyll and two pheophytin molecules. The multimer model[39], in which the transition energies of the six central pigments are assumed to be equal and the couplings between adjacent pigments are similar, proposed the absence of a special pair in the PSII reaction centre. It also suggested that the

BOX 1

Coherent charge separation in reaction centres

Box 1 Fig. (left) depicts the energy level scheme for the bacterial reaction centre, including the coherent motion (red arrows) of the excited-state wave packet from the donor (P^*B_A) to the primary photoproduct ($P^+B_A^-$). In a pump–probe experiment, the initial wave packet is created by the pump and the subsequent dynamics of the excited state are probed by detecting the stimulated emission of the donor and the absorption of the charge-separated product $P^+B_A^-$. The 130 cm^{-1} mode triggers the motion of the wave packet and promotes penetration of the wave packet through the $P^+B_A^-$ potential. A further reorganization of the $P^+B_A^-$ state is induced by the 30 cm^{-1} rotational mode. Notably, although we depict a one-dimensional scheme, the 130 cm^{-1} and 30 cm^{-1} modes are orthogonal to each other.

Box 1 Fig. (right) presents a simplified scheme of coherent energy transfer and primary charge separation in the PSII reaction centre. Subscript notations indicate the central absorption wavelength, and the superscript notations δ+ and δ– indicate charge-transfer character and δ* indicates exciton character.

For the P_{D1} charge-separation pathway, the coherent motion (thick red arrows) of the initial wave packet in the higher exciton state $(P_{D2}P_{D1})_+^*{}_{\approx 660\,nm}$ (orange) and relaxation to the lower exciton–charge-transfer state $(P_{D2}^{\delta+}P_{D1}^{\delta-})_-^*{}_{\approx 675\,nm}$ (pink) is shown. Coherent charge separation leads to the formation of the mixed charge-transfer–exciton state $(P_{D2}^+P_{D1}^-)^{\delta*}{}_{\approx 690\,nm}$ (dark red), which is followed by non-coherent transfer (thin red arrow) to form the final charge-transfer state $P_{D1}^+Phe_{D1}^-$ (green). Note that the intermediate charge-transfer state $P_{D1}^+Chl_{D1}^-$ has been omitted for clarity. Coherent transfers are possible owing to coupling to the 340 cm^{-1} vibrational mode.

For the Chl_{D1} charge-separation pathway, non-coherent transfer (thin blue arrows) from the lowest exciton–charge-transfer state $(Chl_{D1}^{\delta+}Phe_{D1}^{\delta-})^*{}_{\approx 681\,nm}$ (light blue) to the localized (weakly coupled to the exciton manifold) charge-transfer state $Chl_{D1}^+Phe_{D1}^-$ (dark blue) and further transfer to the final charge-transfer state $P_{D1}^+Phe_{D1}^-$ (green) is shown. Coherent transfer (purple arrow) between the exciton–charge-transfer states $(P_{D2}^{\delta+}P_{D1}^{\delta-})_-^*{}_{\approx 675\,nm}$ (pink) and $(Chl_{D1}^{\delta+}Phe_{D1}^{\delta-})^*{}_{\approx 681\,nm}$ (light blue) is indicated. This coherent transfer corresponds to mixing between the two states that is promoted by the 120 cm^{-1} mode and that enables switching between the charge-separation pathways. Wavy black arrows highlight the energy gaps between the exciton and charge-transfer states that are in quasi-resonance with the two vibrational modes, 120 cm^{-1} and 340 cm^{-1}. The participation of the pigments and the location of the charges in the relevant states is superimposed on the X-ray crystal structure of each (adapted from ref. 9). Note that although we have presented a simplified one-dimensional scheme, in reality, the PSII reaction centre has a multidimensional energy landscape in which each state has its own configuration coordinates.

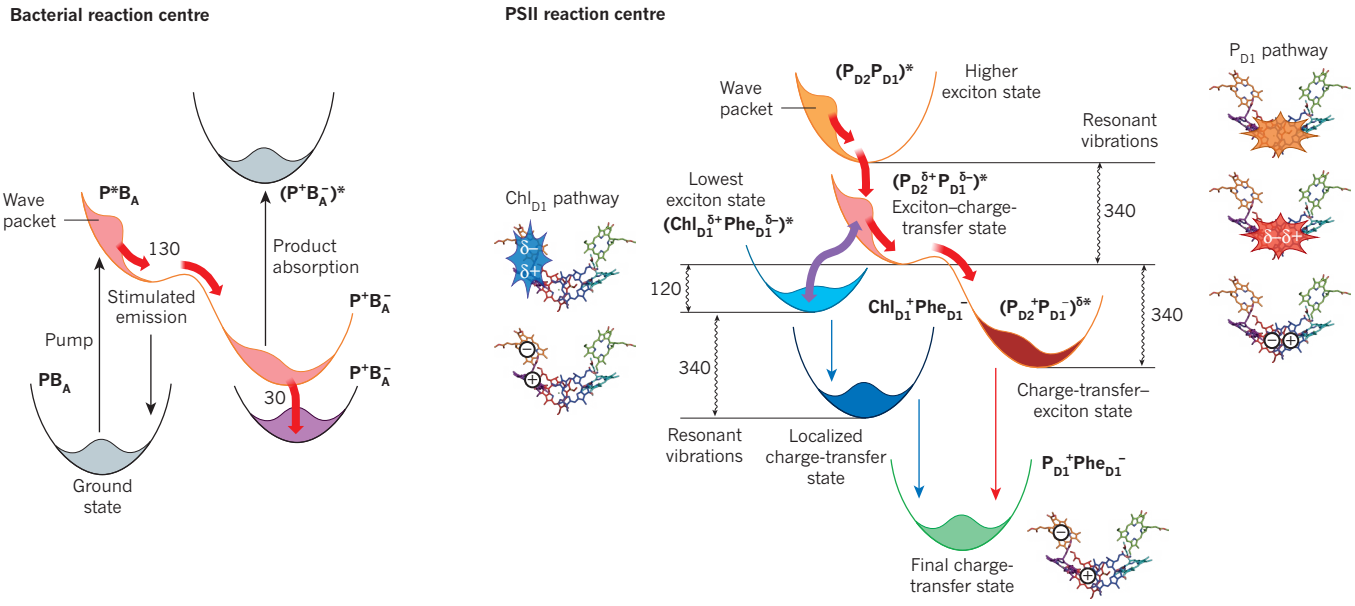

excitation is delocalized over various combinations of neighbouring pigments that depend on the specific realization of the disorder. Although the multimer model enabled a reasonable description (a unified picture) of the spectra and dynamics[41], it did not provide a good quantitative fit of the spectral shapes, owing to its non-realistic assumption about the site energies.

To better understand the energy landscape and dynamics of the PSII reaction centre, there has been a combined experimental and theoretical effort to assign the primary donor P680 to specific chlorophyll molecules or combinations. In 2001, the X-ray structure of PSII was determined at a resolution of 3.8 Å (ref. 7). It revealed the centre-to-centre distance between the central P_{D1} and P_{D2} chlorophyll molecules to be 10.0 Å, which is greater than the equivalent distance (7.8 Å) in the bacterial reaction centre special pair[5] and is consistent with the existence of weaker P_{D1}–P_{D2} coupling in the PSII reaction centre, in line with the multimer model[39]. Determination of the PSII structure in 2004 at a resolution of 3.5 Å (ref. 8) showed a shorter distance (8.2 Å) between P_{D1} and P_{D2}, which supports the existence of a charge-separation scheme in the PSII reaction centre that is similar to that of the bacterial reaction centre, with the central P_{D1} and P_{D2} chlorophylls acting as the primary donor. However, because the coupling of P_{D1} and P_{D2} in the PSII reaction centre is weaker than the coupling of the special pair in the bacterial reaction centre, and because charge separation in the bacterial reaction centre can start from the central special pair bacteriochlorophylls as well as from the accessory bacteriochlorophyll B_A (ref. 31), the discussion about the identity of the primary donor in PSII was prolonged[24,42,43]. The quantitative analysis of several spectral responses at different temperatures[44] and time-resolved spectroscopic

experiments[45,46] provided evidence to show that the accessory Chl_{D1} is the primary electron donor and that Phe_{D1} is the primary electron acceptor. A charge-separation sequence was therefore proposed: $RC^* \rightarrow Chl_{D1}^{+}Phe_{D1}^{-} \rightarrow P_{D1}^{+}Phe_{D1}^{-}$, in which RC^* represents the excited state of the reaction centre that is mainly localized on Chl_{D1}.

A quantitative description of various PSII reaction centre spectroscopic data[26,44,47,48] was facilitated by the use of modified Redfield theory[25], which explicitly includes pigment–pigment (exciton) interactions and coupling to phonons, and gives realistic spectral line shapes and relaxation rates. The site energies of all of the pigments were unambiguously determined by the simultaneous fit of several steady-state spectra: absorption, fluorescence, linear dichroism, circular dichroism and singlet-minus-triplet spectra at different temperatures, as well as the absorption spectra of modified reaction centres such as those with Phe_{D1} or Phe_{D2} modifications or those that lack one Chlz[44,48]. Modified Redfield theory was also used to describe the dynamics of charge separation by modelling time-resolved experimental data[47]. The latter application of the modified Redfield theory[48] includes mixing of the excited states with the charge-transfer states by including the fit of the Stark spectrum, which is sensitive to the energy of the charge-transfer states and the mixing of exciton and charge-transfer states. The best fit was found to correspond to a primary charge-transfer state (that is mixed with the excited states) in the central P_{D1} and P_{D2} chlorophylls ($P_{D2}^{+}P_{D1}^{-}$). This configuration opens the possibility that charge separation may start not only from the previously proposed Chl_{D1} primary donor, but also through direct exciton-type relaxation from the low-energy exciton state that is delocalized over P_{D1} and P_{D2} to the $P_{D2}^{+}P_{D1}^{-}$ charge-transfer state. Notably, the primary $Chl_{D1}^{+}Phe_{D1}^{-}$ charge-transfer state also gave a reasonably good fit to the Stark spectrum. These findings led to the idea of the co-existence of at least two charge-separation pathways in the PSII reaction centre[48].

Two charge–separation pathways

In 2010, the presence of two different charge-separation pathways in the PSII reaction centre was demonstrated experimentally[49], a finding that was supported further by modelling[50]. The experimental data consisted of a detailed transient absorption spectroscopy study: nine experiments (under different excitation conditions) were performed that simultaneously probed all relevant absorption bands (the main band at 680 nm and the Phe_{D1} bands at 545 nm ($Phe_{D1}^{*}/Phe_{D1}^{-}$) and 460 nm ($Phe_{D1}^{-}$)) and monitored all timescales that are relevant to charge separation. The combination of these nine experiments with the application of global and target analysis[51] enabled the two charge-separation pathways of the PSII reaction centre to be determined unambiguously. Another advantage of the modifed Redfield model[48] is its use of a realistic (experimentally determined) spectral density of electron–phonon coupling, which includes coupling to a manifold of high-frequency vibrations. This facilitated the correct estimation of the relaxation dynamics, enabling the quantitative fit of the transient absorption spectra[50].

Mixed exciton–charge–transfer states

Further experimental data has confirmed the presence of two charge-separation pathways in the PSII reaction centre. The application of Stark spectroscopy, which is sensitive to the presence of charge-transfer states, to a series of eight site-directed mutants with modifications that are close to the pigments that are directly involved in charge separation (P_{D1}, P_{D2}, Chl_{D1} and Phe_{D1}) enabled the first determination of the excited states that are capable of initiating charge separation, in terms of pigment composition, central absorption wavelength and charge-transfer character[52]. The two lowest-energy excitons were found to be strongly mixed with the charge-transfer states (as proposed previously, by theory[48]). In other words, the mixed exciton–charge-transfer state exhibits a non-uniform electron density distribution. Consequently, the observed charge-transfer state has exciton character. This mixing creates channels for ultrafast charge separation owing to the similarity between the electronic-density distribution of the reactant (an exciton state with charge-transfer character, known as the exciton–charge-transfer state) and the product (a charge-transfer state with exciton character, known as the charge-transfer–exciton state) of the charge-separation reaction. The states that are capable of starting charge separation are shown in Box 1 and the observed charge-separation pathways[30,49,52] are:

$$(Chl_{D1}^{\delta+}Phe_{D1}^{\delta-})^{*}_{\approx 681\,nm} \rightarrow Chl_{D1}^{+}Phe_{D1}^{-} \rightarrow P_{D1}^{+}Phe_{D1}^{-}$$

for the Chl_{D1} pathway and

$$(P_{D2}^{\delta+}P_{D1}^{\delta-}Chl_{D1})^{*}_{\approx 675\,nm} \rightarrow (P_{D2}^{+}P_{D1}^{-})^{\delta*}_{\approx 690\,nm} \rightarrow P_{D1}^{+}Chl_{D1}^{-} \rightarrow P_{D1}^{+}Phe_{D1}^{-}$$

for the P_{D1} pathway,

in which the wavelength values indicate the central absorption wavelength, δ+ and δ– indicate charge-transfer character and δ* indicates exciton character. Because the charge-transfer states are optically dark and have not yet been observed spectroscopically[53], no central wavelength is indicated. Given that the participation of Chl_{D1} in the $(P_{D2}^{\delta+}P_{D1}^{\delta-}Chl_{D1})^{*}_{\approx 675\,nm}$ state is small, for clarity, we omit Chl_{D1} from this state in the text that follows. The observed Phe_{D1}^{-} formation occurs on both sub-picosecond and picosecond timescales; whereas the sub-picosecond formation is described by the Chl_{D1} pathway, the picosecond formation can be explained only by the P_{D1} pathway[49,50]. As a result, the identity of the primary electron donor could finally be solved. P680 is not a single entity as both $(Chl_{D1}^{\delta+}Phe_{D1}^{\delta-})^{*}_{\approx 681\,nm}$ and $(P_{D2}^{\delta+}P_{D1}^{\delta-})^{*}_{\approx 675\,nm}$ can act as the donor, depending on the specific realization of the disorder. We therefore propose that the term P680 is abandoned for several reasons: one of the electron donors absorbs at around 675 nm rather than around 680 nm; the donor is not just one state; and, most importantly, the term P680 is an oversimplification and is therefore incorrect. For investigations that do not deal with the early events of charge separation, we suggest that the term RC^* is used instead of $P680^*$. And to describe the site of cation stabilization, P_{D1}^{+} should be used in place of $P680^{+}$.

Dynamic coherence reveals functional inner coherence

By 2012, the precursor states, pathways and timescales of charge separation had been identified. However, the precise mechanism that is responsible for the high efficiency of charge separation remained unknown. One plausible mechanism is the presence of quantum delocalization in the states that are involved in charge separation. This proposal was triggered by the observation of long-lived electronic and electron-vibrational coherences in light-harvesting complexes[54–62], as well as in oxidized bacterial reaction centres that are unable to perform charge separation[63,64].

The coherences that were observed in photosynthetic complexes by two-dimensional electronic spectroscopy as oscillations in signal amplitude[57,65] correspond to dynamic coherence between the electronic states (excitons, exciton–charge-transfer states or charge-transfer states) of the system. This dynamic coherence is created only on excitation with laser light, which is coherent and ultrafast, and cannot be produced in natural photosynthesis, which operates under illumination with sunlight, which is incoherent and non-ultrafast. However, the presence of long-lived dynamic coherence is a signature of inner (steady-state) coherence (coherent mixing within electronic states), which leads to the delocalization of excitation energy over several pigments or states, including charge-transfer states. This delocalization is an intrinsic and time-independent property of the system that is operational in natural photosynthesis, which means that it has a strong influence on the promotion of high-speed and efficient charge separation in reaction centres. In particular, primary charge separation can be sped up by vibration-assisted delocalization between the excited electron donor and the first charge-transfer state (as explained in Fig. 2). Delocalization enables a directed transfer along several pathways in space[66], which produces the conversion of excitation energy on ultrafast timescales

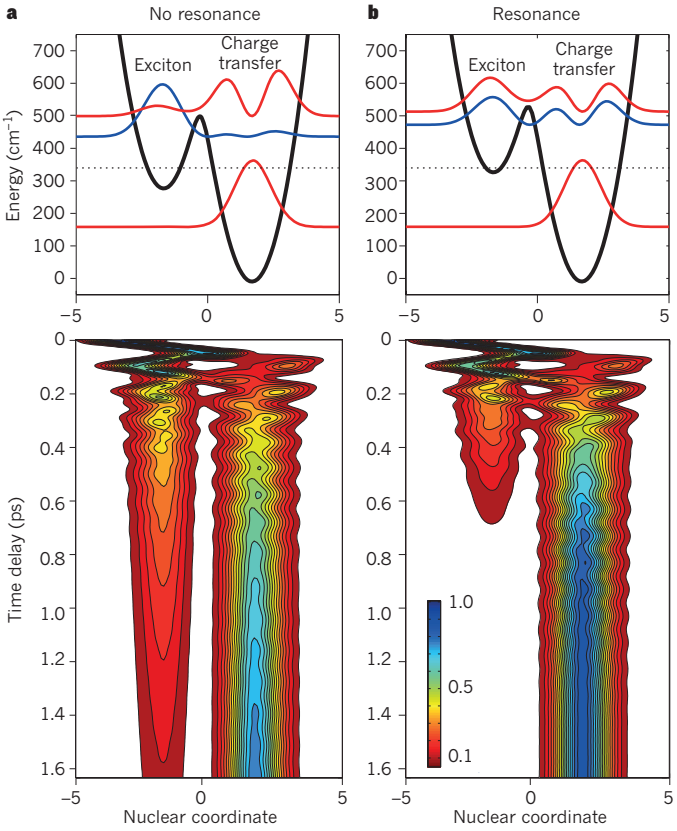

Figure 2 | Resonant vibrations promote effective charge separation. a, **b**, The effect of the absence (**a**) or presence (**b**) of resonance between a vibrational mode and the energy gap between exciton and charge-transfer states on electron-vibrational mixing (top panels) and charge-separation dynamics (bottom panels). This electron-vibrational resonance in the one-dimensional, two-state case is based on a numerical example presented in ref. 78 but recalculated with slightly different parameters. The nuclear coordinate (*x* axis of all panels, using the same scale) represents a collective nuclear coordinate in a multidimensional configuration space that describes the coupling of the electronic excitation to many nuclear modes (such as phonons and vibrations). Coupling between the diabatic electronic states is 150 cm^{-1}. The dimensionless displacement in nuclear coordinates for the non-mixed diabatic state is –1.7 for the exciton and 1.7 for the charge-transfer state. (Mixing induces a slight shift from these values.) The displacement of the ground state is –3.4. The dynamics are calculated using Redfield theory in the exciton-vibrational basis at 77 K. The potential wells (black lines, top panels) represent the mixed wells for the exciton (left well) and the charge-transfer state (right well), which are coupled to a 340 cm^{-1} vibrational mode (this energy level is indicated by a dashed black line). Blue and red lines show the vibronic wavefunctions of the exciton and the charge-transfer state, respectively. In the non-resonant case (**a**, top), with an energy gap of 290 cm^{-1}, the vibronic wavefunctions do not overlap, and the exciton and the charge-transfer state remain mostly localized in their own potential well. Yet in the resonant case (**b**, top), with an energy gap of 340 cm^{-1}, the vibronic wavefunctions do overlap, and the exciton and the charge-transfer state become mixed and delocalized over both potential wells. Mixing has a dramatic effect on the dynamics of electron transfer from the exciton to the charge-transfer state (bottom panels). Impulsive excitation of the exciton state creates a wave packet that oscillates between the potential wells of the exciton and the charge-transfer state with a 100-fs period, which corresponds to the 340 cm^{-1} vibrational mode. The time-dependent shape of the vibronic wave packet (normalized to unity) is shown by the heat map (coloured scale, inset). Localization of the wave packet at the bottom of the potential well is associated with the relative population of a state. In the non-resonant case (**a**, bottom), the wave packet takes 2.3 ps to create a significant population of the charge-transfer state. But in the resonant case (**b**, bottom), the penetration of the wave packet into the charge-transfer state is 3.3-fold faster, and it takes 0.7 ps to achieve a significant population of this state. This difference, by preventing back transfers, provides the charge-separation reaction with directionality and efficiency. Adapted from ref. 78 with permission from the PCCP Owner Societies.

and makes these processes less sensitive to energetic disorder, avoiding energy losses and providing efficiency.

The observation of long-lived dynamic coherence in photosynthetic complexes is remarkable because these complexes are warm, wet and noisy; therefore, in principle, no sustained dynamic coherence was expected to survive in such a fluctuating environment. The long-lived character of the observed coherences was initially proposed to arise from the coupling of vibrations to the electronic states, which is known as the vibration-assisted electronic (vibronic) coherent mechanism[67–76].

Coherence in the PSII reaction centre

Indeed, by combining the results of the two-dimensional electronic spectroscopy experiment and Redfield theory, it has been demonstrated that long-lived dynamic coherence is present in the PSII reaction centre at physiological temperature (277 K) and that there is a strong correlation between the degree of inner coherence and the efficiency of charge separation[77–79]. The dynamic coherence observed is active during charge separation for at least 1 ps at both physiological temperature[77] and cryogenic temperature (77 K)[77,80]. The vibronic coherent mechanism[77–80] promotes the functionally relevant inner coherence in the PSII reaction centre. In this mechanism, matching of a pigment's intramolecular vibrational mode with the energy differences that exist between the exciton and the charge-transfer states (or between charge-transfer states) promotes mixing of the zero-phonon level of the electron donor with the first vibrational sub-level of the acceptor. This mixing produces vibronic states that are delocalized over the two electronic states (Fig. 2), which speeds up electron transfer from donor to acceptor[78,79].

In the PSII reaction centre, the dominant vibrational modes of chlorophyll, as observed by two-dimensional electronic spectroscopy, are 120 cm^{-1}, 340 cm^{-1} and 730 cm^{-1} (±20 cm^{-1}) (ref. 77). Depending on the degree of exciton mixing within these coherences, they can be classified as electronic (120 cm^{-1}), mixed electron-vibrational (340 cm^{-1}) or purely vibrational (730 cm^{-1})[78,79] (Box 2). The 120 cm^{-1} mode mixes the two lowest-energy exciton–charge-transfer states, $(P_{D2}{}^{\delta+}P_{D1}{}^{\delta-})^*_{\approx 675\,nm}$ and $(Chl_{D1}{}^{\delta+}Phe_{D1}{}^{\delta-})^*_{\approx 681\,nm}$, and effectively delocalizes the initial excitation over these states, which promotes switching between the P_{D1} and Chl_{D1} pathways (Box 1 and Fig. 2). This mixing and the resulting delocalization has crucial consequences for the functionality of the PSII reaction centre: it enables the system to simultaneously sample the Chl_{D1} and P_{D1} charge-separation pathways and to therefore select the most optimal pathway in accordance with the specific realization of the disorder. The 340 cm^{-1} mode promotes energy and electron transfer between the states $(P_{D2}P_{D1})^*_{+\,\approx 660\,nm}$, $(P_{D2}{}^{\delta+}P_{D1}{}^{\delta-})^*_{-\,\approx 675\,nm}$ and $(P_{D2}{}^{+}P_{D1}{}^{-})^{\delta *}_{\approx 690\,nm}$. The dynamic coherence between these states is observed in two-dimensional electronic spectroscopy as quantum beats with a frequency of around 340 cm^{-1}. The electron-vibrational resonance mixing of the excited and charge-transfer states that contribute to these states promotes ultrafast and efficient charge separation (Fig. 2). The 730 cm^{-1} mode has a higher energy than most exciton splittings. This coherence is therefore mainly vibrational, which means that it corresponds to a wave-packet motion along an individual excited state potential and does not have a considerable role in the charge-separation process.

Design principles

A combination of the knowledge obtained on the PSII reaction centre by spectroscopic experiments and modified Redfield theory has changed our understanding of light-driven photosynthetic charge separation. The PSII reaction centre has found several complementary and interrelated solutions to ensure that almost 100% efficiency is achieved in charge separation, as well as to avoid energy losses, which are the expected consequence of its intrinsically disordered energy landscape. The disorder problem is probably the same as those found in sustainable and affordable energy-conversion systems that are based on abundant materials. Current knowledge on the mechanisms of charge separation can be summarized by four principles that aim to provide a guide for

BOX 2

Types of coherence

● **Electronic coherence** Pigment–pigment coupling produces a manifold of exciton states that are delocalized over a combination of pigments (Box 2 Fig., top left). Numbers 1, 2 and 3 represent pigments, the top three horizontal black lines represent exciton states and the size of the black circles represents the participation ratio of the pigments in each exciton. The magenta, green and blue bands show the absorption lineshapes of the individual exciton states; the amplitudes are proportional to the transition dipole strength of each exciton. Coherent superposition of elementary pigment excitations in a collective exciton state (or inner coherence) can be reached by the selective excitation of individual exciton states. Non-selective (broadband) excitation of several excitons (blue arrows) produces a coherent superposition of these exciton states (blue ring). This gives rise to dynamic coherence, which creates a localized wave packet (grey bands) that oscillates (red arrow) between the sites involved in the excited collective states with a period that corresponds to the energy splitting between these exciton energy levels. Wave-packet motion is visualized as amplitude oscillations of, for instance, the transient absorption or the two-dimensional electronic-spectroscopy signal.

The 120 cm^{-1} two-dimensional frequency map of the PSII reaction center (Box 2 Fig., bottom left; reproduced from ref. 77), which contains a peak below the diagonal (cross-peak), is shown as an example of mainly electronic coherence[78,79]. Red areas correspond to the maximum signal amplitude and dark blue regions correspond to zero amplitude. The vertical and horizontal displacements from the diagonal of the cross-peak are equal to the energy of the vibrational quantum, which is 120 cm^{-1} in this case.

● **Mixed electron-vibrational coherence** Exciton mixing of two electronic states that are coupled to a vibrational mode results in a complicated manifold of electron-vibrational (vibronic) states (Box 2 Fig., top centre). The potential wells (curved lines) for the excited state 1 (top left) and the excited state 2 (top right), as well as the ground state (bottom) are shown. The blue curves indicate diabatic (non-mixed) potentials whereas the red curves indicate the exciton state (mixed) potentials. The magenta and green bands represent the absorption lineshapes of the individual vibronic states, with amplitudes proportional to the transition dipole strength of each state. Each vibronic state is a superposition of the vibrational sublevels of the two states. The vibronic wavefunctions in magenta have a predominant contribution of state 1, whereas those in green have a predominant contribution of state 2. Coherent excitation of several vibronic levels produces a wave packet (grey bands) that is localized in the nuclear and electronic coordinate (real space). (The initial wave packet is localized in site 1.) The coherent motion of this wave packet (red arrow) determines both the electronic and vibrational amplitude oscillations of the two-dimensional electronic-spectroscopy signal.

The 340 cm^{-1} two-dimensional frequency map of the PSII reaction center (Box 2 Fig., bottom centre; reproduced from ref. 77) exemplifies mixed vibronic coherence[78,79]. This map shape emerges when the vibrational frequency is in resonance with the energy gap of the electronic states. Although it resembles the map for vibrational coherence (see Box 2 Fig., bottom right), the most intense cross-peak exhibits an increased amplitude owing to the contribution of vibronic mixing between the electronic states[78,79]. The vertical and horizontal displacements from the diagonal of the most intense cross-peaks are equal to the energy of the vibrational quantum, which is 340 cm^{-1} here.

● **Vibrational coherence** Vibrational states that are associated with a pigment's ground state (bottom potential well) and excited states (top well) are delocalized over the effective nuclear coordinates (Box 2 Fig., top right). The magenta, green and cyan bands represent the absorption lineshapes of the individual vibrational states, with amplitudes proportional to the transition dipole strength of each state. Coherent excitation of many vibrational sublevels produces a vibrational wave packet (grey bands) that localizes near the boundary of the excited-state potential well, which oscillates (red arrow) in the potential energy surface with a period that corresponds to the energy difference between the vibrational sublevels.

The 730 cm^{-1} two-dimensional frequency map of the PSII reaction centre (Box 2 Fig., bottom right; reproduced from ref. 77) exemplifies vibrational coherence[78,79]. This map shape emerges when the oscillating frequency is far from that of the energy gaps of the electronic states. Pure vibrational coherence produces the chair-type structure, which has an intense diagonal component and weak cross-peak components[78,79]. The vertical and horizontal displacements from the diagonal of the most intense cross-peaks are equal to the energy of the vibrational quantum, which is 730 cm^{-1} here.

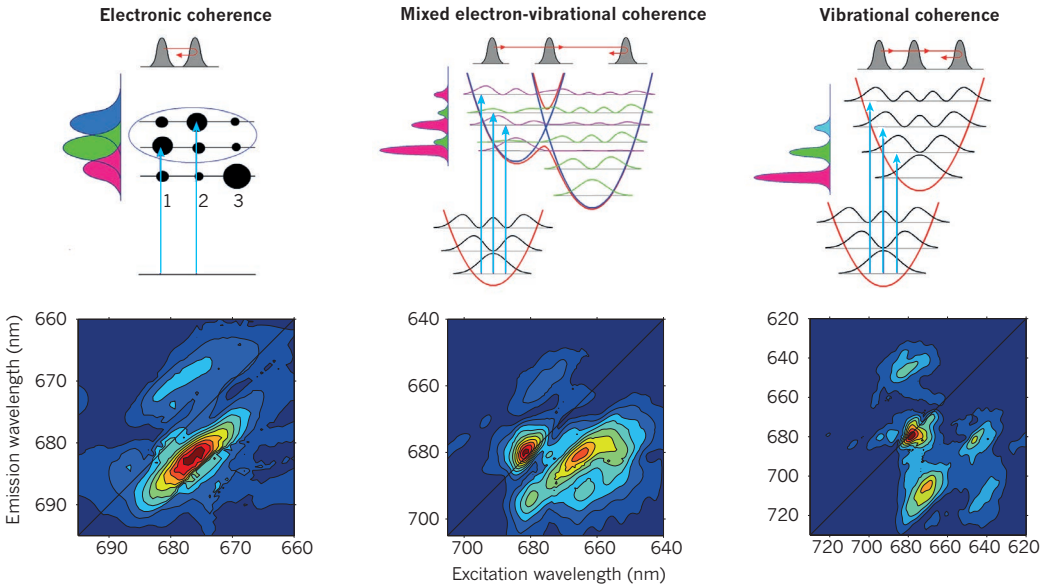

the design and construction of robust and efficient human-made energy conversion systems.

The mixing of exciton states with charge–transfer states

Charge separation in the photosynthetic reaction centre (after long-range migration of excitation energy in the light-harvesting antenna) should be irreversible to prevent back transfers to the antenna, in which the excitation could be lost or trapped. To compete with back transfers, the charge-separation event, which starts with a high-energy exciton state and relaxes to a dynamically localized low-energy charge-transfer state, must be as fast as possible. The quasi-classical energy 'hopping' between non-mixed excitons and charge-transfer states is slow enough[81] to enable back transfer to the antenna. In principle, a quantum superposition (or mixing) of the two states can create much faster transfers from the exciton to the charge-transfer state. However, overlap of the zero-phonon levels of the exciton and the charge-transfer state is minimal, owing to the strong displacement along nuclear coordinates of the charge-transfer zero-phonon state, which is the result of the strong coupling of the charge-transfer state to phonons. Consequently, the mixing of the electron donor and acceptor is not so pronounced, even when there is strong electrostatic coupling between them.

Resonant vibrations

Exciton–charge-transfer mixing can be dramatically enhanced in the presence of an intramolecular vibrational quantum with an energy that is close to the energy gap between the exciton and charge-transfer states. The involvement of a resonant vibration promotes the exciton–charge-transfer interaction owing to the mixing of the electronic zero-phonon origin of the exciton with a vibrational sublevel of the charge-transfer state, which creates the non-classical penetration of the exciton into the charge-transfer potential and speeds up charge transfer (Fig. 2). Although this is the case for the PSII reaction centre, so far, there is no experimental evidence to support such electron-vibrational resonance in the bacterial reaction centre. As well as the mixing between pigments or between the exciton and charge-transfer states, strong coupling to vibrations inseparably mixes the Q_x and Q_y transitions in chlorophyll *a* pigments[82], which therefore changes the polarization of the lowest Q_y band and affects the steady-state pigment–pigment or exciton–charge-transfer coherences. We note that the vibration-assisted coherent mechanism is less important for the transfer of energy between pure exciton states in the light-harvesting antenna because the relative displacements between these states are not as large as those between the exciton and charge-transfer states. Therefore, the overlap between the zero-phonon levels of the antenna excitons is optimized for the efficient transfer of energy, even in the absence of vibration-assisted mixing.

Control of charge separation by the smart protein matrix

The protein conformation-induced modulation of the energy gaps between states that creates and destroys the mixing of the exciton and charge-transfer states enables switching between charge-separation pathways. The possibility of using more than one pathway increases the probability of having at least one effective channel of charge transfer in a disordered system, which provides functional flexibility and avoids the trapping of excitation in unproductive states. Notably, the coherent exciton–charge-transfer mixing that is assisted by vibrations occurs within states (inner coherence) and therefore increases the rate of charge separation in a particular direction (that corresponds to a particular pathway), not only on coherent excitation but also in natural photosynthesis.

Control of vibronic coherence by the smart protein matrix

The exciton–charge-transfer mixing that is controlled by the smart protein matrix promotes the fast and efficient formation of the charge-transfer state. However, this formation must be irreversible to avoid back transfer to the antenna. Both initial coherence and subsequent decoherence (or dephasing) are therefore needed for efficient charge transfer. The protein matrix is characterized by a rich manifold of vibrational modes, some of which it uses to create the fast coherent population of the charge-transfer state. The remaining modes induce dephasing that stabilizes the primary charge-transfer photoproduct. In the bacterial reaction centre, a special mode was found to stabilize the photoproduct: the 30 cm^{-1} mode that was assigned to the rotation of a water molecule that is located between the special pair P and the accessory bacteriochlorophyll B_A (ref. 33). Other modes might also contribute to dephasing and reorganization in the charge-transfer potential. In the PSII reaction centre, no specific modes with responsibility for dephasing have been found. The dephasing and dynamic localization in the primary charge-transfer state are probably a result of the simultaneous action of many phonon or vibrational modes. We propose that the coupling of specific vibrations to electronic states, both for coherence and decoherence, may be a general strategy that is used in nature to selectively drive an electronic process and to provide directionality[83].

The quantum design principles that are active in photosynthetic reaction centres are connected to the phenomenon of inner coherence, which leads to delocalization (including the vibration-assisted delocalization of electronic states) that increases the effectiveness of charge separation, not only on coherent and impulsive laser excitation that is used in two-dimensional electronic spectroscopy, but also on non-coherent, non-impulsive solar illumination under natural conditions. We therefore propose that the four design principles that we have discussed can be applied to the development of new solar-energy technologies.

Application of the design principles

A human-made energy conversion system should fulfil several requirements to exploit the benefits of the design principles of charge separation that we present. We propose a bio-inspired approach that aims to understand the mechanisms that promote the desired functionality so that the underpinning natural design principles can be implemented in human-made systems. This approach enables and requires researchers to develop innovative and creative strategies for translating these natural principles into those that can be applied to human-made systems and that have the potential to adapt the functionality of the natural system to the requirements of people and can even outperform nature, in terms of stability and robustness.

So far, several elegant and promising approaches have been presented for photovoltaic or solar-to-electricity (dye-sensitized solar cells[84,85] and other (organic)-photovoltaic systems[86]) and solar-to-fuel (artificial leaf[87]) energy conversion. In all of these systems, energy losses that result from the charge recombination of the initial excitons, the charge-transfer state or the charge-separated state are caused mainly by energetic disorder in the materials that they comprise. This issue can be overcome by applying the design principles that are presented in this Review, including delocalization[88,89] and resonant vibrations[88,90,91], by promoting the rapid forward and irreversible transfer of energy and electrons in disordered systems.

Basic elements

Two elements are required for the design and construction of a bio-inspired charge-separation unit: chromophores (light-absorbing and charge-separating molecules) and a matrix that maintains the position of the chromophores and tunes their electronic properties. To maximize the absorption of solar light, chromophores must have high absorption coefficients and a broad absorption range, requirements that are usually achieved through conjugated molecules such as porphyrins, chlorins, carotenes, bilins, quinones and flavins. Combinations of chromophores can be used to absorb an even broader range of the solar spectrum. The selected chromophores should also be able to participate in energy and electron transfer processes. Furthermore, the vibrational structure of the chromophores should be taken into account to incorporate the required resonance between exciton–charge-transfer energy gaps and the vibrations of the chromophores. The matrix should contain specific

sites to bind the chromophores through chromophore–matrix interactions, either covalently or non-covalently. It should also be rigid enough to maintain the chromophore–chromophore interactions that are created but sufficiently flexible to enable certain levels of static disorder so that the energy gaps between chromophores fluctuate slightly, which facilitates a higher probability of exciton–charge-transfer resonance with specific vibrational modes. Such a matrix could be attained by supramolecular structures[92] such as organogels[93] or other polymers, DNA origami[94] or synthetic proteins[95].

Excitons and charge-transfer states

To promote and control excitonic interactions between chromophores, the position of the chromophores with respect to each other, which refers to the distance between and the relative orientation of their transition dipole moments, should be carefully chosen to obtain the desired energy landscape. For example, the head-to-tail and sandwich configurations are relative orientations in a dimer that give rise to different energy landscapes (see ref. 11 for a detailed explanation of the excitonic dimer properties). The advantages of creating excitons are numerous and include: the generation of broader absorption bands owing to spreading of the excitonic transitions; faster energy transfer from high- to low-energy states through exciton relaxation in clusters of strongly coupled chromophores; faster migration between delocalized exciton states from other clusters; fewer energy- or electron-transfer steps to reach the final state; and robustness against local minima owing to delocalization. Although the generation of broader absorption bands increases the energy that is available, the other advantages reduce the probability of energy loss.

The required charge-transfer states can be created by modifying the electronic distribution of the chromophores by means of specific interactions with their environment, which includes nearby chromophores or the matrix. For instance, the electron density around the chromophores can be modified by introducing charges, hydrogen bonds or dispersive interactions (through a polarizable environment). The strategy that involves the insertion of hydrogen bonds has proved effective in increasing the oxidation–reduction midpoint potential of the special pair in the bacterial reaction centre[27,29].

Exciton–charge-transfer mixing by resonant vibrations

The vibrational spectrum of the chromophore has a crucial role in promoting the mixing of excitons with charge-transfer states. Selected intramolecular vibrations should match the difference in energy that exists between the excitons and charge-transfer states and therefore couple strongly to the relevant electronic states.

Control of charge-separation pathways by the smart matrix

After several mixed exciton–charge-transfer states have been engineered into the system, inevitably, a number of charge-separation pathways will emerge. Although this means that the desired multiple-pathways principle has been achieved, special care should be taken to avoid back reactions (by stabilizing the product state[17]) and to avoid unproductive charge-separation pathways.

Control of vibronic coherence by the smart matrix

When introducing a chromophore into a matrix, it should be taken into account that chromophore–chromophore interactions as well as chromophore–matrix interactions modify the electronic and vibrational energy levels of the chromophore. We propose to determine the energy landscape of and to investigate the presence of delocalization, exciton–charge-transfer mixing and electron-vibrational matching in the human-made energy conversion system by applying absorption spectroscopy, linear dichroism and circular dichroism, fluorescence spectroscopy, Stark spectroscopy and two-dimensional electronic spectroscopy. If delocalization, exciton–charge-transfer mixing and electron-vibrational matching are all present, the system would be expected to perform charge separation on an ultrafast timescale and with high efficiency. However, if any of these features have not been accomplished, further interactions should be included or new chromophores should be selected.

Devices for solar-energy conversion

After an efficient bio-inspired charge-separation unit has been designed and constructed, the holes and electrons that are created should be harvested for use. In the solar-to-electricity approach to energy conversion, the charge-separation unit should be connected to electrodes to collect the electrons that are generated on the absorption of light. We note that this is not a trivial procedure, owing to, for instance, the presence of competing charge-separation pathways at the PSII–electrode interface[96]. Furthermore, the solar-to-electricity approach is affected by two main problems: the intermittency of solar light (little or no light is available during the night or on cloudy days) and storage of the energy that is generated.

We therefore propose the solar-to-fuel approach, which goes one step further than the solar-to-electricity method: it provides a fuel that contains solar energy stored in chemical bonds in a liquid or a gas that can be efficiently stored and transported for later use[97]. To that end, the charge-separation unit must be coupled to catalysts to drive the splitting of water (at the oxidation site) and the production of a fuel (at the reduction site). This approach imposes one constraint on the charge-separation unit: the oxidation–reduction midpoint potential of the oxidation and reduction sites should fulfil the respective requirements of driving the oxidation of water and generating the fuel, as well as overcome the overpotential that is imposed by each of the catalysts. Another complexity of this approach resides in the fact that the timescales of ultrafast charge separation and slower catalysis must be synchronized.

The next steps

One of the biggest challenges for the field of quantum biology is to investigate and demonstrate whether non-trivial quantum effects have an essential role in fundamental processes such as the transfer of energy, electrons, hydrides and proton-coupled electrons, as well as in photoisomerization reactions. These processes form the basis of photosynthesis, catalysis, the sense of vision and the sense of smell; all hold fundamental relevance as well as great promise for technological applications.

In photosynthesis, specifically, two next steps are evident. The first will be to demonstrate experimentally whether coherence correlates with efficiency, for instance, by applying two-dimensional electronic spectroscopy to mutants[98] of various charge-separation efficiencies and disrupted resonance between electronic states and pigment vibrations. And the second will be to study larger and more intact photosynthetic supercomplexes, or even whole photosynthetic bacterial cells[99,100], to investigate whether coherence can extend over large distances.

Other directions for research include the investigation of the role of coherence in existing human-made solar-energy conversion systems such as photovoltaic or nanophotonic devices. Last, but not least, it is of vital importance that human-made energy conversion systems are designed and constructed on the basis of the quantum design principles of photosynthesis that we have presented in this Review. ■

Received 18 July 2016; accepted 31 January 2017.

1. Blankenship, R. E. *Molecular Mechanisms of Photosynthesis* (Blackwell Science, 2002).
2. Beddard, G. S. & Porter, G. Concentration quenching in chlorophyll. *Nature* **260,** 366–367 (1976).
3. Myers, J. A. The 1932 experiments. *Photosynth. Res.* **40,** 303–310 (1994).
4. van Grondelle, R. & van Gorkom, H. The birth of the photosynthetic reaction center: the story of Lou Duysens. *Photosynth. Res.* **120,** 3–7 (2014).
5. Deisenhofer, J., Epp, O., Miki, K., Huber, R. & Michel, H. X-ray structure-analysis of a membrane-protein complex: electron-density map at 3 Å resolution and a model of the chromophores of the photosynthetic reaction center from *Rhodopseudomonas viridis*. *J. Mol. Biol.* **180,** 385–398 (1984).
6. Koepke, J. *et al.* pH modulates the quinone position in the photosynthetic reaction center from *Rhodobacter sphaeroides* in the neutral and charge separated states. *J. Mol. Biol.* **371,** 396–409 (2007).

7. Zouni, A. *et al.* Crystal structure of photosystem II from *Synechococcus elongatus* at 3.8 Å resolution. *Nature* **409,** 739–743 (2001).
8. Ferreira, K. N., Iverson, T. M., Maghlaoui, K., Barber, J. & Iwata, S. Architecture of the photosynthetic oxygen-evolving center. *Science* **303,** 1831–1838 (2004).
9. Umena, Y., Kawakami, K., Shen, J.-R. & Kamiya, N. Crystal structure of oxygen-evolving photosystem II at a resolution of 1.9 Å. *Nature* **473,** 55–60 (2011).
This paper presents the crystal structure of PSII at atomic resolution.
10. Scholes, G. D., Fleming, G. R., Olaya-Castro, A. & van Grondelle, R. Lessons from nature about solar light harvesting. *Nature Chem.* **3,** 763–774 (2011).
11. van Amerongen, H., Valkunas, L. & van Grondelle, R. *Photosynthetic Excitons* (World Scientific, 2000).
This book proposes the concept of the disordered photosynthetic exciton model.
12. Frenkel, J. On the transformation of light into heat in solids. I. *Phys. Rev.* **37,** 17–44 (1931).
13. Durrant, J. R. *et al.* Subpicosecond equilibration of excitation energy in isolated photosystem II reaction centers. *Proc. Natl Acad. Sci. USA* **89,** 11632–11636 (1992).
14. Zinth, W. & Wachtveitl, J. The first picoseconds in bacterial photosynthesis: ultrafast electron transfer for the efficient conversion of light energy. *ChemPhysChem* **6,** 871–880 (2005).
15. Rappaport, F. & Diner, B. A. Primary photochemistry and energetics leading to the oxidation of the $(Mn)_4Ca$ cluster and to the evolution of molecular oxygen in photosystem II. *Coord. Chem. Rev.* **252,** 259–272 (2008).
16. Croce, R. & van Amerongen, H. Light-harvesting and structural organization of photosystem II: from individual complexes to thylakoid membrane. *J. Photochem. Photobiol. B* **104,** 142–153 (2011).
17. Rutherford, A. W., Osyczka, A. & Rappaport, F. Back-reactions, short-circuits, leaks and other energy wasteful reactions in biological electron transfer: redox tuning to survive life in O_2. *FEBS Lett.* **586,** 603–616 (2012).
18. Steffen, M. A., Lao, K. & Boxer, S. G. Dielectric asymmetry in the photosynthetic reaction center. *Science* **264,** 810–816 (1994).
19. Amesz, J. & Hoff, A. J. *Biophysical Techniques in Photosynthesis* Vol. 3 (Kluwer Academic, 1996).
20. Berera, R., Van Grondelle, R. & Kennis, J. T. M. Ultrafast transient absorption spectroscopy: principles and application to photosynthetic systems. *Photosynth. Res.* **101,** 105–118 (2009).
21. Schlau-Cohen, G. S., Dawlaty, J. M. & Fleming, G. R. Ultrafast multidimensional spectroscopy: principles and applications to photosynthetic systems. *IEEE J. Sel. Top. Quantum Electron.* **18,** 283–295 (2012).
22. Shkuropatov, A. Y. *et al.* Reaction centers of photosystem II with a chemically-modified pigment composition: exchange of pheophytins with 13^1-deoxo-13^1-hydroxy-pheophytin *a*. *FEBS Lett.* **450,** 163–167 (1999).
23. Vacha, F. *et al.* Photochemistry and spectroscopy of a five-chlorophyll reaction center of photosystem II isolated by using a Cu affinity column. *Proc. Natl Acad. Sci. USA* **92,** 2929–2933 (1995).
24. Diner, B. A. *et al.* Site-directed mutations at D1-His198 and D2-His197 of photosystem II in *Synechocystis* PCC 6803: sites of primary charge separation and cation triplet stabilization. *Biochemistry* **40,** 9265–9281 (2001).
25. Zhang, W. M., Meier, T., Chernyak, V. & Mukamel, S. Exciton migration and three-pulse femtosecond optical spectroscopies of photosynthetic antenna complexes. *J. Chem. Phys.* **108,** 7763–7774 (1998).
26. Raszewski, G., Diner, B. A., Schlodder, E. & Renger, T. Spectroscopic properties of reaction center pigments in photosystem II core complexes: revision of the multimer model. *Biophys. J.* **95,** 105–119 (2008).
27. Allen, J. P. & Williams, J. C. in *The Biophysics of Photosynthesis* (eds Golbeck, J. H. & van der Est, A.) 275–295 (Springer, 2014).
28. Wydrzynski, T. J. & Satoh, K. *Photosystem II: The Light-Driven Water:Plastoquinone Oxidoreductase* (Springer, 2005).
29. Allen, J. P. *et al.* Effects of hydrogen bonding to a bacteriochlorophyll–bacteriopheophytin dimer in reaction centers from *Rhodobacter sphaeroides*. *Biochemistry* **35,** 6612–6619 (1996).
30. Romero, E., Novoderezhkin, V. I. & van Grondelle, R. in *Quantum Effects in Biology* (eds Mohseni, M., Omar, Y., Engel, G. S. & Plenio, M. B.) 179–197 (Cambridge Univ. Press, 2014).
31. van Brederode, M. E., Jones, M. R., van Mourik, F., van Stokkum, I. H. M. & van Grondelle, R. A new pathway for transmembrane electron transfer in photosynthetic reaction centers of *Rhodobacter sphaeroides* not involving the excited special pair. *Biochemistry* **36,** 6855–6861 (1997).
This paper reveals the discovery of multiple pathways for charge separation in the bacterial reaction centre.
32. Vos, M. H., Rappaport, F., Lambry, J.-C., Breton, J. & Martin, J.-L. Visualization of coherent nuclear motion in a membrane protein by femtosecond spectroscopy. *Nature* **363,** 320–325 (1993).
This paper shows that vibrational wave packets form in bacterial reaction centres after they are excited with a femtosecond laser pulse.
33. Yakovlev, A. G., Shkuropatov, A. Y. & Shuvalov, V. A. Nuclear wave packet motion between P* and $P^+B_A^-$ potential surfaces with a subsequent electron transfer to H_A in bacterial reaction centers at 90 K. Electron transfer pathway. *Biochemistry* **41,** 14019–14027 (2002).
34. Novoderezhkin, V. I., Yakovlev, A. G., Van Grondelle, R. & Shuvalov, V. A. Coherent nuclear and electronic dynamics in primary charge separation in photosynthetic reaction centers: a Redfield theory approach. *J. Phys. Chem. B* **108,** 7445–7457 (2004).
This article describes coherent vibrational and electronic dynamics during charge separation in bacterial reaction centers.
35. Danielius, R. V. *et al.* The primary reaction of photosystem II in the D1–D2–cytochrome *b*-559 complex. *FEBS Lett.* **213,** 241–244 (1987).
36. Bosch, M. K., Proskuryakov, I. I., Gast, P. & Hoff, A. J. Relative orientation of the optical transition dipole and triplet axes of the photosystem II primary donor. A magnetophoto-selection study. *J. Phys. Chem.* **99,** 15310–15316 (1995).
37. Konermann, L. & Holzwarth, A. R. Analysis of the absorption spectrum of photosystem II reaction centers: temperature dependence, pigment assignment and inhomogeneous broadening. *Biochemistry* **35,** 829–842 (1996).
38. Tetenkin, V. L., Gulyaev, B. A., Seibert, M. & Rubin, A. B. Spectral properties of stabilized D1/D2/cytochrome *b*-559 photosystem II reaction center complex. *FEBS Lett.* **250,** 459–463 (1989).
39. Durrant, J. R. *et al.* A multimer model for P680, the primary electron donor of photosystem II. *Proc. Natl Acad. Sci. USA* **92,** 4798–4802 (1995).
This paper proposes the original multimer model for the PSII reaction centre.
40. Peterman, E. J. G., van Amerongen, H., van Grondelle, R. & Dekker, J. P. The nature of the excited state of the reaction center of photosystem II of green plants: a high-resolution fluorescence spectroscopy study. *Proc. Natl Acad. Sci. USA* **95,** 6128–6133 (1998).
41. Renger, T. & Marcus, R. A. Photophysical properties of PS-2 reaction centers and a discrepancy in exciton relaxation times. *J. Phys. Chem. B* **106,** 1809–1819 (2002).
42. Dekker, J. P. & van Grondelle, R. Primary charge separation in photosystem II. *Photosynth. Res.* **63,** 195–208 (2000).
43. Prokhorenko, V. I. & Holzwarth, A. R. Primary processes and structure of the photosystem II reaction center: a photon echo study. *J. Phys. Chem. B* **104,** 11563–11578 (2000).
44. Raszewski, G., Saenger, W. & Renger, T. Theory of optical spectra of photosystem II reaction centers: location of the triplet state and the identity of the primary electron donor. *Biophys. J.* **88,** 986–998 (2005).
45. Groot, M. L. *et al.* Initial electron donor and acceptor in isolated photosystem II reaction centers identified with femtosecond mid-IR spectroscopy. *Proc. Natl Acad. Sci. USA* **102,** 13087–13092 (2005).
46. Holzwarth, A. R. *et al.* Kinetics and mechanism of electron transfer in intact photosystem II and in the isolated reaction center: pheophytin is the primary electron acceptor. *Proc. Natl Acad. Sci. USA* **103,** 6895–6900 (2006).
47. Novoderezhkin, V. I., Andrizhiyevskaya, E. G., Dekker, J. P. & van Grondelle, R. Pathways and timescales of primary charge separation in the photosystem II reaction center as revealed by simultaneous fit of time-resolved fluorescence and transient absorption. *Biophys. J.* **89,** 1464–1481 (2005).
48. Novoderezhkin, V. I., Dekker, J. P. & van Grondelle, R. Mixing of exciton and charge-transfer states in photosystem II reaction centers: modeling of Stark spectra with modified Redfield theory. *Biophys. J.* **93,** 1293–1311 (2007).
49. Romero, E., van Stokkum, I. H. M., Novoderezhkin, V. I., Dekker, J. P. & van Grondelle, R. Two different charge separation pathways in photosystem II. *Biochemistry* **49,** 4300–4307 (2010).
This article reveals the discovery of two pathways for charge separation in the PSII reaction centre.
50. Novoderezhkin, V. I., Romero, E., Dekker, J. P. & van Grondelle, R. Multiple charge separation pathways in photosystem II: modeling of transient absorption kinetics. *ChemPhysChem* **12,** 681–688 (2011).
51. van Stokkum, I. H. M., Larsen, D. S. & van Grondelle, R. Global and target analysis of time-resolved spectra. *Biochim. Biophys. Acta* **1657,** 82–104 (2004).
52. Romero, E. *et al.* Mixed exciton-charge-transfer states in photosystem II: Stark spectroscopy on site-directed mutants. *Biophys. J.* **103,** 185–194 (2012).
53. Reimers, J. R. *et al.* Challenges facing an understanding of the nature of low-energy excited states in photosynthesis. *Biochim. Biophys. Acta* **1857,** 1627–1640 (2016).
54. Savikhin, S., Buck, D. R. & Struve, W. S. Oscillating anisotropies in a bacteriochlorophyll protein: evidence for quantum beating between exciton levels. *Chem. Phys.* **223,** 303–312 (1997).
55. Brixner, T. *et al.* Two-dimensional spectroscopy of electronic couplings in photosynthesis. *Nature* **434,** 625–628 (2005).
56. Zigmantas, D. *et al.* Two-dimensional electronic spectroscopy of the B800–B820 light-harvesting complex. *Proc. Natl Acad. Sci. USA* **103,** 12672–12677 (2006).
57. Engel, G. S. *et al.* Evidence for wavelike energy transfer through quantum coherence in photosynthetic systems. *Nature* **446,** 782–786 (2007).
This paper presents the first observation of quantum dynamics in photosynthesis.
58. Calhoun, T. R. *et al.* Quantum coherence enabled determination of the energy landscape in light-harvesting complex II. *J. Phys. Chem. B* **113,** 16291–16295 (2009).
59. Collini, E. *et al.* Coherently wired light-harvesting in photosynthetic marine algae at ambient temperature. *Nature* **463,** 644–647 (2010).
60. Panitchayangkoon, G. *et al.* Long-lived quantum coherence in photosynthetic complexes at physiological temperature. *Proc. Natl Acad. Sci. USA* **107,** 12766–12770 (2010).
61. Schlau-Cohen, G. S. *et al.* Elucidation of the timescales and origins of quantum electronic coherence in LHCII. *Nature Chem.* **4,** 389–395 (2012).
62. Hildner, R., Brinks, D., Nieder, J. B., Cogdell, R. J. & van Hulst, N. F. Quantum coherent energy transfer over varying pathways in single light-harvesting complexes. *Science* **340,** 1448–1451 (2013).
63. Lee, H., Cheng, Y. C. & Fleming, G. R. Coherence dynamics in photosynthesis: protein protection of excitonic coherence. *Science* **316,** 1462–1465 (2007).
64. Westenhoff, S., Palecek, D., Edlund, P., Smith, P. & Zigmantas, D. Coherent picosecond exciton dynamics in a photosynthetic reaction center. *J. Am. Chem. Soc.* **134,** 16484–16487 (2012).

65. Collini, E. Spectroscopic signatures of quantum-coherent energy transfer. *Chem. Soc. Rev.* **42,** 4932–4947 (2013).
66. Cheng, Y. C. & Fleming, G. R. Dynamics of light harvesting in photosynthesis. *Annu. Rev. Phys. Chem.* **60,** 241–262 (2009).
67. Prior, J., Chin, A. W., Huelga, S. F. & Plenio, M. B. Efficient simulation of strong system-environment interactions. *Phys. Rev. Lett.* **105,** 050404 (2010).
68. Womick, J. M. & Moran, A. M. Vibronic enhancement of exciton sizes and energy transport in photosynthetic complexes. *J. Phys. Chem. B* **115,** 1347–1356 (2011).
69. Kolli, A., Nazir, A. & Olaya-Castro, A. Electronic excitation dynamics in multichromophoric systems described via a polaron-representation master equation. *J. Chem. Phys.* **135,** 154112 (2011).
70. Christensson, N., Kauffmann, H. F., Pullerits, T. & Mancal, T. Origin of long-lived coherences in light-harvesting complexes. *J. Phys. Chem. B* **116,** 7449–7454 (2012).
71. Chin, A. W., Huelga, S. F. & Plenio, M. B. Coherence and decoherence in biological systems: principles of noise-assisted transport and the origin of long-lived coherences. *Phil. Trans. R. Soc. A* **370,** 3638–3657 (2012).
72. Kolli, A., O'Reilly, E. J., Scholes, G. D. & Olaya-Castro, A. The fundamental role of quantized vibrations in coherent light harvesting by cryptophyte algae. *J. Chem. Phys.* **137,** 174109 (2012).
This article demonstrates the role of discrete and quantized vibrations in photosynthetic light harvesting.
73. Butkus, V., Zigmantas, D., Valkunas, L. & Abramavicius, D. Vibrational vs. electronic coherences in 2D spectrum of molecular systems. *Chem. Phys. Lett.* **545,** 40–43 (2012).
74. Chin, A. W. *et al.* The role of non-equilibrium vibrational structures in electronic coherence and recoherence in pigment-protein complexes. *Nature Phys.* **9,** 113–118 (2013).
75. Tiwari, V., Peters, W. K. & Jonas, D. M. Electronic resonance with anticorrelated pigment vibrations drives photosynthetic energy transfer outside the adiabatic framework. *Proc. Natl Acad. Sci. USA* **110,** 1203–1208 (2013).
76. O'Reilly, E. J. & Olaya-Castro, A. Non-classicality of the molecular vibrations assisting exciton energy transfer at room temperature. *Nature Commun.* **5,** 3012 (2014).
77. Romero, E. *et al.* Quantum coherence in photosynthesis for efficient solar-energy conversion. *Nature Phys.* **10,** 676–682 (2014).
This paper presents the discovery of quantum coherence in charge separation in the PSII reaction centre and is the first to correlate coherence with the efficiency of charge separation.
78. Novoderezhkin, V. I., Romero, E. & van Grondelle, R. How exciton-vibrational coherences control charge separation in the photosystem II reaction center. *Phys. Chem. Chem. Phys.* **17,** 30828–30841 (2015).
79. Novoderezhkin, V. I., Romero, E., Prior, J. & van Grondelle, R. Exciton-vibrational resonance and dynamics of charge separation in the photosystem II reaction center. *Phys. Chem. Chem. Phys.* **19,** 5195–5208 (2017).
80. Fuller, F. D. *et al.* Vibronic coherence in oxygenic photosynthesis. *Nature Chem.* **6,** 706–711 (2014).
81. Novoderezhkin, V. I. & van Grondelle, R. Physical origins and models of energy transfer in photosynthetic light harvesting. *Phys. Chem. Chem. Phys.* **12,** 7352–7365 (2010).
82. Reimers, J. R. *et al.* Assignment of the Q-bands of the chlorophylls: coherence loss via Q_x–Q_y mixing. *Sci. Rep.* **3,** 2761 (2013).
83. Ishizaki, A. & Fleming, G. R. Theoretical examination of quantum coherence in a photosynthetic system at physiological temperature. *Proc. Natl Acad. Sci. USA* **106,** 17255–17260 (2009).
84. O'Regan, B. & Gratzel, M. A low-cost, high-efficiency solar cell based on dye-sensitized colloidal TiO_2 films. *Nature* **353,** 737–740 (1991).
85. Hagfeldt, A., Boschloo, G., Sun, L., Kloo, L. & Pettersson, H. Dye-sensitized solar cells. *Chem. Rev.* **110,** 6595–6663 (2010).
86. Polman, A., Knight, M., Garnett, E. C., Ehrler, B. & Sinke, W. C. Photovoltaic materials: present efficiencies and future challenges. *Science* **352,** aad4424 (2016).
87. Liu, C., Colón, B. C., Ziesack, M., Silver, P. A. & Nocera, D. G. Water splitting-biosynthetic system with CO_2 reduction efficiencies exceeding photosynthesis. *Science* **352,** 1210–1213 (2016).
88. Bredas, J.-L., Sargent, E. H. & Scholes, G. D. Photovoltaic concepts inspired by coherence effects in photosynthetic systems. *Nature Mater.* **16,** 35–44 (2017).
89. Bakulin, A. A. *et al.* The role of driving energy and delocalized states for charge separation in organic semiconductors. *Science* **335,** 1340–1344 (2012).
90. Falke, S. M. *et al.* Coherent ultrafast charge transfer in an organic photovoltaic blend. *Science* **344,** 1001–1005 (2014).
91. De Sio, A. *et al.* Tracking the coherent generation of polaron pairs in conjugated polymers. *Nature Commun.* **7,** 13742 (2016).
92. Ramamurthy, V. & Inoue, Y. *Supramolecular Photochemistry: Controlling Photochemical Processes* (Wiley, 2011).
93. Ajayaghosh, A., Praveen, V. K. & Vijayakumar, C. Organogels as scaffolds for excitation energy transfer and light harvesting. *Chem. Soc. Rev.* **37,** 109–122 (2008).
94. Pinheiro, A. V., Han, D., Shih, W. M. & Yan, H. Challenges and opportunities for structural DNA nanotechnology. *Nature Nanotechnol.* **6,** 763–772 (2011).
95. Moser, C. C. *et al.* in *Methods in Enzymology* Vol. 580 (ed. Pecoraro, V. L.) 365–388 (Academic, 2016).
96. Zhang, J. Z. *et al.* Competing charge transfer pathways at the photosystem II–electrode interface. *Nature Chem. Biol.* **12,** 1046–1052 (2016).
97. Ringsmuth, A. K., Landsberg, M. J. & Hankamer, B. Can photosynthesis enable a global transition from fossil fuels to solar fuels, to mitigate climate change and fuel-supply limitations? *Renew. Sustain. Energy Rev.* **62,** 134–163 (2016).
98. Flanagan, M. L. *et al.* Mutations to *R. sphaeroides* reaction center perturb energy levels and vibronic coupling but not observed energy transfer rates. *J. Phys. Chem. A* **120,** 1479–1487 (2016).
99. Dahlberg, P. D. *et al.* Coherences observed *in vivo* in photosynthetic bacteria using two-dimensional electronic spectroscopy. *J. Chem. Phys.* **143,** 101101 (2015).
100. Dostál, J., Pšenčík, J. & Zigmantas, D. *In situ* mapping of the energy flow through the entire photosynthetic apparatus. *Nature Chem.* **8,** 705–710 (2016).

Acknowledgements E.R. and R.v.G. were supported by: the VU University Amsterdam; the Laserlab-Europe consortium; TOP grant 700.58.305 from the Foundation of Chemical Sciences, part of Netherlands Organisation for Scientific Research (NWO); European Research Council Advanced Grant 267333 (PHOTPROT); and the European Union FP7 project PAPETS (grant agreement 323901). R.v.G. gratefully acknowledges his Academy Professorship from the Netherlands Royal Academy of Sciences and was also supported by the Canadian Institute for Advanced Research. V.I.N. was supported by the Russian Foundation for Basic Research (grant number 15-04-02136) and by an NWO visitor grant.

Author Information Reprints and permissions information is available at www.nature.com/reprints. The authors declare no competing financial interests. Readers are welcome to comment on the online version of this paper at go.nature.com/2mtsbek. Correspondence should be addressed to E.R. (eli@few.vu.nl).

Reviewer Information *Nature* thanks J. Minagawa and the other anonymous reviewer(s) for their contribution to the peer review of this work.